

Geophysical Research Letters

RESEARCH LETTER

10.1029/2020GL091830

Key Points:

- Magnetosonic waves can extend above the lower hybrid resonance frequency in the off-equatorial high-density plasmasphere
- The near-equatorial instabilities of hot protons are difficult to explain the observed frequency extension of magnetosonic waves
- The unusual magnetosonic waves are more likely to grow accumulatively over latitudes $|\lambda| < 30^\circ$ during the bounce-drift propagation

Supporting Information:

- Supporting Information S1

Correspondence to:

Z. Su and N. Liu,
szpe@mail.ustc.edu.cn;
toshpro@mail.ustc.edu.cn

Citation:

Wu, Z., Su, Z., Liu, N., Gao, Z., Zheng, H., Wang, Y., & Wang, S. (2021). Off-equatorial source of magnetosonic waves extending above the lower hybrid resonance frequency in the inner magnetosphere. *Geophysical Research Letters*, 48, e2020GL091830. <https://doi.org/10.1029/2020GL091830>

Received 24 NOV 2020

Accepted 13 FEB 2021

Off-Equatorial Source of Magnetosonic Waves Extending Above the Lower Hybrid Resonance Frequency in the Inner Magnetosphere

Zhiyong Wu^{1,2,3} , Zhenpeng Su^{1,2} , Nigang Liu^{1,2,3} , Zhonglei Gao⁴ , Huinan Zheng^{1,2} , Yuming Wang^{1,2} , and Shui Wang^{1,2}

¹Department of Geophysics and Planetary Sciences, CAS Key Laboratory of Geospace Environment, University of Science and Technology of China, Hefei, China, ²CAS Center for Excellence in Comparative Planetology, University of Science and Technology of China, Hefei, China, ³Anhui Mengcheng Geophysics National Observation and Research Station, University of Science and Technology of China, Hefei, China, ⁴School of Physics and Electronic Sciences, Changsha University of Science and Technology, Changsha, China

Abstract Inner magnetospheric magnetosonic waves are usually considered to grow from the near-equatorial ion Bernstein instability below the lower hybrid resonance frequency and contribute significantly to the radiation belt electron dynamics. We here present unusual observations of magnetosonic waves extending above the local lower hybrid resonance frequency in the midlatitude $\sim 15^\circ$ plasmasphere after the substorm proton injection. Linear instability analyses and ray-tracing simulations show that, because of the latitudinal variation of normal angles, these waves have little growth near the equator but are amplified accumulatively to the observable level over broad latitudes $|\lambda| < 30^\circ$ during the bounce-drift propagation. Our data and modeling illustrate a previously unexplored scenario that off-equatorial proton ring distributions could be a significant source of magnetosonic waves in the inner magnetosphere. Such off-equatorially generated magnetosonic waves might differ from the near-equatorially generated ones in latitudinal coverage, wavevector distribution, and then effect on the radiation belt electrons.

Plain Language Summary Magnetosonic waves refer to the nearly linearly polarized, compressional, electromagnetic emissions in the inner magnetosphere. They have recently received an increased interest for their contributions to the Van Allen radiation belt electron dynamics. A fundamental question has been where and how the magnetosonic waves are generated. In contrast to the traditional view that magnetosonic waves grow from ion Bernstein instability near the magnetic equator, we here propose the possibility of off-equatorial sources for magnetosonic waves on the basis of the analysis of the unusual magnetosonic waves extending above the local lower hybrid resonance frequency in the midlatitude plasmasphere. Our modeling shows that these waves have little growth near the equator but are amplified accumulatively to the observable level by substorm-injected protons over latitudes $|\lambda| < 30^\circ$ during the bounce-drift propagation. Because of the differences in latitudinal coverage and wavevector distribution, the off-equatorially and near-equatorially generated magnetosonic waves are expected to have different effects on the radiation belt electrons.

1. Introduction

In the inner magnetosphere, magnetosonic waves phenomenologically refer to the nearly linearly polarized, compressional, electromagnetic emissions (Boardsen, Gallagher, et al., 1992; Perraut et al., 1982; Russell et al., 1970; Tsurutani et al., 2014). One school of thought is that they grow from the Bernstein instability of velocity ring distributions of hot protons injected from the plasmashet (Boardsen, Gallagher, et al., 1992; Chen, Thorne, Jordanova, & Horne, 2010; Curtis & Wu, 1979; Gary et al., 2010; Gulelmi et al., 1975). For a sufficient cold plasma background, the ion Bernstein mode couples to the magnetosonic-whistler mode (Chen, 2015; Gary et al., 2010; K. Liu et al., 2011). After the theoretical works (Bortnik & Thorne, 2010; Horne, Thorne, et al., 2007; Shprits, 2009) highlighting the contribution of magnetosonic waves to the radiation belt electron dynamics, the generation, propagation, and distribution of these waves have received much attention in recent years.

Magnetosonic waves are usually detected within $\pm 5^\circ$ latitude away from the equator and below the lower hybrid resonance frequency (Boardsen, Hospodarsky, Kletzing, et al., 2016; Ma, Li, Bortnik, et al., 2019; Meredith et al., 2008; Němec et al., 2005; Yuan et al., 2019). These near-equatorially confined waves are commonly considered to grow spontaneously around the equator, with the growth rates peaking at the quasi-perpendicular normal angles (Gary et al., 2010; K. Liu et al., 2011; Ma, Li, Chen, et al., 2014; Min & Liu, 2015). They are able to bounce near the equator and propagate over a broad range of radial and azimuthal distances, as shown by ray-tracing simulations (Chen & Thorne, 2012; Horne, Wheeler, & Alleyne, 2000; Kasahara et al., 1994; Santolík et al., 2016; Xiao, Zhou, et al., 2012) and multi-point observations (Santolík, Pickett, Gurnett, Maksimovic, & Cornilleau-Wehrlin, 2002; Su et al., 2017).

According to Liouville's theorem, the velocity ring distributions of hot protons should exist over a broad range of latitudes along the field lines (e.g., Boardsen, Gallagher, et al., 1992). Whether the off-equatorial proton rings can effectively promote the growth of magnetosonic waves remains unclear. There have been reports of magnetosonic waves far away from the equator (Boardsen, Hospodarsky, Kletzing, et al., 2016; Ni et al., 2018; Tsurutani et al., 2014; Zhima et al., 2015) or above the lower hybrid resonance frequency (Boardsen, Hospodarsky, Kletzing, et al., 2016). This gives rise to at least two possibilities. One possibility is these waves originate from the near-equatorial instability. The waves capable of reaching higher latitudes should have wavevectors deviating more significantly from the perpendicular direction at the equatorial source region (Figure 5 of Zhima et al., 2015). Above the lower hybrid resonance frequency, the wavevectors have to fall out of the resonance cone determined by $\tan^2 \psi_{\text{res}} = -P/S$ (Stix, 1962) particularly at the equator with relatively weak magnetic fields. However, according to previous simulations for the observed proton distributions (e.g., Su et al., 2017), there is little growth associated with intermediate normal angles for the magnetosonic waves. Another possibility is these waves grow mainly in the off-equatorial region where the wavevectors have become close to the perpendicular direction. This possibility is explored in this letter.

We here report the unusual observations by Van Allen Probes (Mauk et al., 2013) of the magnetosonic waves extending above the local lower hybrid resonance frequency in the off-equatorial plasmasphere. On the basis of wave and particle observations, linear instability calculations and ray-tracing simulations, we show that these waves likely originated from the off-equatorial region and grew accumulatively to the observable level during the bounce-drift propagation.

2. Van Allen Probes Observations

The Van Allen Probes mission, formerly known as the Radiation Belt Storm Probes (RBSP) mission (Mauk et al., 2013), comprises two probes in the slightly different elliptical Earth orbits with the apogees $\sim 6 R_E$ and the perigees $\sim 0.1 R_E$ (R_E is the Earth radii). Because of the low orbital inclination of $\sim 10^\circ$, the Van Allen Probes made only $\sim 15\%$ measurements at latitudes $|\lambda| > 15^\circ$ in the inner magnetosphere (Mauk et al., 2013). We here use the data from the Electric and Magnetic Field Instrument and Integrated Science suite (EMFISIS; Kletzing et al., 2013), the Helium Oxygen Proton Electron Mass Spectrometer (HOPE; Funsten et al., 2013) of the Energetic particle, Composition and the Thermal plasma suite (ECT; Spence et al., 2013), and the Radiation Belt Storm Probes Ion Composition Experiment (RBSPICE; Mitchell et al., 2013) onboard the Van Allen Probes mission. Specifically, the tri-axial search coil magnetometer (MAG) of EMFISIS detected the in situ magnetic fields; the High Frequency Receiver (HFR) of EMFISIS measured the upper hybrid resonance frequency, allowing the derivation of cold electron density (Kurth et al., 2014); the Waveform Receiver (WFR) of EMFISIS provided the electromagnetic power spectra of waves from 2 Hz to 12 kHz; HOPE and RBSPICE sampled the proton fluxes from ~ 1 eV to ~ 400 keV.

Figure 1 shows an overview of the unusual magnetosonic wave event observed by the twin spacecraft of Van Allen Probes mission on August 13, 2013. Within the time period of interest, the magnetosphere was free from storms (with $\text{SYM-H} > -10$ nT) but affected by strong substorms (with AE reaching up to 600 nT). During the outbound passes ($L > 5.2$) after $\sim 19:05$ UT, both probes encountered the energy-dispersive injection of hot protons in the duskside sector. In response to the enhancement of > 1 keV protons, intense electromagnetic waves centering near the local lower hybrid resonance frequency were detected in the off-equatorial ($\lambda \sim 15^\circ$) plasmasphere ($N_e > 100 \text{ cm}^{-3}$), and became unobservable outside the plasmopause (characterized by an obvious decrease in the cold electron density around 20:00 UT in Figures 1b and 1g).

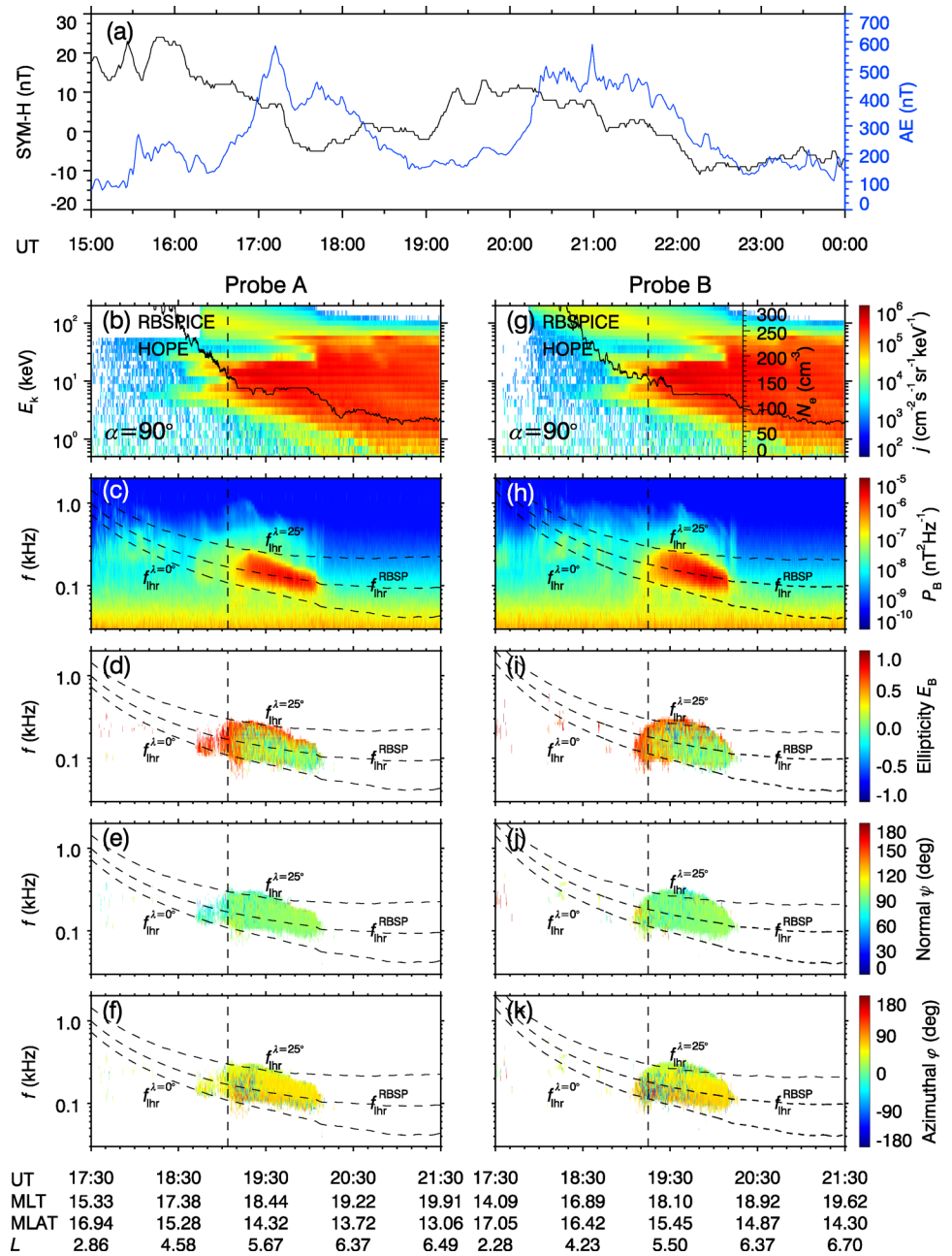


Figure 1. Overview of the unusual magnetosonic wave event observed by Van Allen Probes on August 13, 2013: (a) Geomagnetic indices SYM-H (black) and AE (blue); (b and g) proton differential flux j at the pitch angle $\alpha = 90^\circ$ (color-coded), with the electron density N_e overlaid as the black solid line; (c and h) magnetic power spectral density P_B (color-coded), with the lower hybrid resonance frequency at $\lambda = 25^\circ$, $f_{\text{thr}}^{\lambda=25^\circ}$, at the probe $f_{\text{thr}}^{\text{RBSP}}$ and at the equator $f_{\text{thr}}^{\lambda=0^\circ}$ overlaid as three black dashed lines; (d and i) magnetic ellipticity E_B ; (e and j) wave normal angle ψ defined as the angle between the wavevector and the magnetic field; (f and k) wave azimuthal angle φ defined in the plane perpendicular to the magnetic field, with 90° , -90° , $\pm 180^\circ$, and 0° for the projected wavevectors pointing westward, eastward, earthward, and anti-earthward directions, respectively. Note that near the boundary of magnetosonic wave bands, the polarization information might have been contaminated by the coexisting plasmaspheric hiss waves.

Applying the singular value decomposition technique to the electromagnetic spectral matrices (Santolík, Pickett, Gurnett, & Storey, 2002, 2003), we find that these intense waves had the nearly linear polarizations $E_B \sim 0$ and the quasi-perpendicular and westward-pointing wavevectors (with normal angles $|\psi - 90^\circ| < 10^\circ$ and azimuthal angles $\varphi = 40^\circ - 90^\circ$). Therefore, we identify these waves as the off-equatorial magnetosonic

waves excited by hot protons. The magnetosonic waves were accompanied by the weak hiss waves in the plasmasphere, similar to the situation reported by (Tsurutani et al., 2014). The transverse field contamination by the coexisting plasmaspheric hiss and the phase error between electric and magnetic measurements could have significantly distorted the derivation of azimuthal angles φ of magnetosonic waves, as discussed by Boardsen, Hospodarsky, Min, et al. (2018).

Boardsen, Hospodarsky, Kletzing, et al. (2016) briefly mentioned the existence of magnetosonic waves above the lower hybrid resonance frequency. We here present the first detailed investigation of magnetosonic waves substantially extending above the local lower hybrid resonance frequency $f_{\text{thr}}^{\text{RBSP}}$ in the midlatitude $\sim 15^\circ$ plasmasphere. In the high-density region ($f_{\text{pe}} \gg f_{\text{ce}}$), the lower hybrid resonance frequency is approximated as $f_{\text{thr}} \approx \sqrt{f_{\text{ce}} f_{\text{cp}}}$, with the electron plasma frequency f_{pe} and the gyrofrequencies of electrons f_{ce} and protons f_{cp} . Assuming that the geomagnetic field is scaled by the TS04 model (Tsyganenko & Sitnov, 2005), we can estimate the lower hybrid resonance frequencies at different latitudes along the field lines. In the frequency-time spectrograms, the intense magnetosonic waves are roughly bounded between the lower hybrid resonance frequencies at the equator $f_{\text{thr}}^{\lambda=0^\circ}$ and at the latitude $\lambda = 25^\circ$ $f_{\text{thr}}^{\lambda=25^\circ}$. Such a frequency extension implies, under the cold plasma approximation, a significant deviation of wavevectors from the perpendicular direction even at the observer ($\lambda \sim 15^\circ$) and then the ability of waves to reach higher latitudes. These unusual observations prompt us to reconsider the possibility of off-equatorial amplification of magnetosonic waves in the inner magnetosphere.

3. Latitude-Dependent Instability of Magnetosonic Waves

We evaluate the linear growth rates of magnetosonic waves at different latitudes along the magnetic field lines using our previously developed code (N. Liu et al., 2018a, 2018b; Su et al., 2018) based on the approach of Kennel (1966) and Chen, Thorne, Jordanova, and Horne (2010). Our code does not include the nonresonant growth process proposed by Chen (2015) for magnetosonic waves exactly at $\psi = 90^\circ$. There are mainly three inputs: (1) the magnetic field magnitude scaled by the TS04 model (Tsyganenko & Sitnov, 2005); (2) the field-aligned cold plasma density modeled by Denton et al. (2002)

$$N_e = N_{\text{eq}} \cos^{-2\eta} \lambda \quad (1)$$

with the latitudinal index $\eta = 0.5$ near $L = 5.5$ in the plasmasphere and the equatorial density N_{eq} derived from the in situ measurements; (3) the proton phase space density (Figure S1), which consists of a series of the smooth cubic spline approximations (Reinsch, 1967) of the measurements along the pitch-angle direction at the observer and then is mapped to other latitudes along the field lines according to Liouville's theorem (expediently involving the smooth cubic spline extrapolation near 90° pitch angle at latitudes below the observer). At an arbitrary point in the pitch angle-energy space, the phase space density and its derivatives are obtained through the two-dimensional B-spline fitting (De Boor, 1977).

Because of the close proximity of the two spacecraft, we make the data-to-model comparison for Probe A only (Figure 2). As shown in Figure 2b and Figure S1, the modeled proton phase space densities agree reasonably well with available data at different times (L -shells) and latitudes. Figures 2d, 2f, 2h, and 2j plot the growth rates at latitudes of $\lambda = 0^\circ, 14.3^\circ, 25^\circ$, and 30° with the normal angles $86.3^\circ, 88.0^\circ, 89.8^\circ$, and 89.8° , respectively. In general, the linear growth rates of magnetosonic waves tend to increase as the normal angles approach 90° . When the local lower hybrid resonance frequency at low latitudes is below the upper cutoff frequency of magnetosonic waves, we perform calculations at the resonant angle ψ_{res} ; otherwise, in the absence of nonresonant treatment (Chen, 2015), we select the normal angle $\psi = 89.8^\circ$ for calculations. Around 19:30 UT, Probe A observed the magnetosonic waves whose upper frequency cutoff had the largest positive deviation (Figure 2a) from the local lower hybrid resonance frequency $f_{\text{thr}}^{\text{RBSP}}$. At the equator ($\lambda = 0^\circ$) and the observer ($\lambda \approx 15^\circ$), the corresponding resonant angles are about 86.3° and 88.0° (Figures 2c and 2e). With the normal angles far away from 90° , the obtained growth of waves is allowed from slightly below $f_{\text{thr}}^{\lambda=25^\circ}$ to frequencies much lower than observations and the growth rates are at a quite low level ($K_i \sim 10^{-8} \text{ m}^{-1}$). At higher latitudes, the strong growth of waves tends to occur at higher frequencies. As the

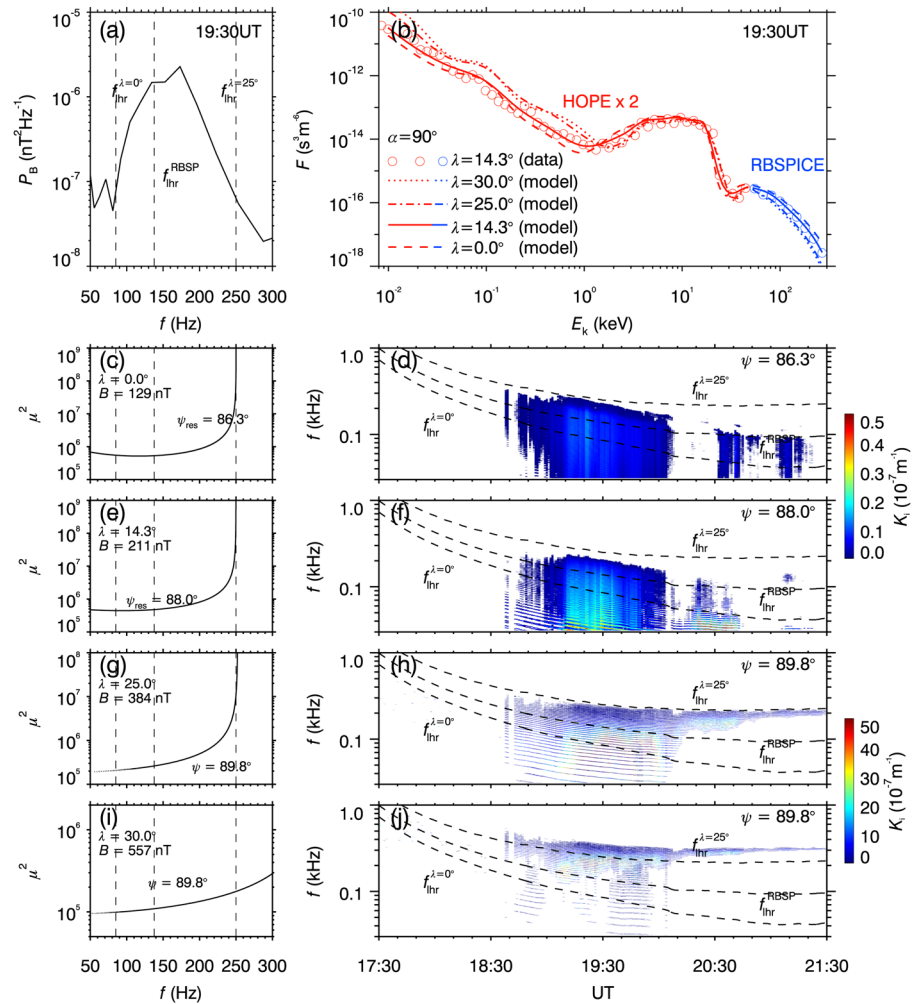


Figure 2. Latitudinal dependence of linear instability: (a) magnetic power spectral density P_B from 50 to 300 Hz observed by Probe A at 19:30 UT, with $f_{\text{thr}}^{\lambda=0^\circ}$, $f_{\text{thr}}^{\text{RBSP}}$ and $f_{\text{thr}}^{\lambda=25^\circ}$ overplotted as the vertical black dashed lines; (b) energy-dependent proton phase space density F at $\alpha = 90^\circ$ observed (circles) by Probe A and modeled (lines) at different latitudes (dashed, solid, dash-dotted and dotted lines for $\lambda = 0^\circ, 14.3^\circ, 25^\circ$, and 30° , respectively); frequency-dependence of the square of the refractive index μ^2 for magnetosonic waves (c) at $\lambda = 0.0^\circ$ with $\psi = \psi_{\text{res}} = 86.3^\circ$, (e) at $\lambda = 14.3^\circ$ with $\psi = \psi_{\text{res}} = 88.0^\circ$, (g) at $\lambda = 25.0^\circ$ with $\psi = 89.8^\circ$ and (i) at $\lambda = 30.0^\circ$ with $\psi = 89.8^\circ$; (d, f, h, j) convective growth rate K_i (color-coded) at the corresponding latitudes and normal angles. In Figure 2b, following previous studies (e.g., Kistler et al., 2016; Min et al., 2018), the HOPE data have been multiplied by 2 (red) to match the RBSPICE data (blue).

normal angle increases to $\psi = 89.8^\circ$ at $\lambda = 25^\circ$ and 30° (Figures 2g and 2i), the modeled waves can have the peak growth rate of $5 \times 10^{-6} \text{ m}^{-1}$ above $f_{\text{thr}}^{\lambda=0^\circ}$. These calculations imply that the off-equatorial amplification could be indispensable for these unusual magnetosonic waves.

In the calculations above, the specific normal angles are not extracted from the available measurements but simply selected according to the dispersion relation of waves with the extreme frequency extension around 19:30 UT. At a different time with a different upper frequency cutoff of waves, the allowed normal angles would vary to some extent. With the propagation effect, the allowed normal angles would deviate further from 90° particularly at latitudes below the observer. As pointed out by an anonymous referee, the actual instability of hot protons would produce waves within a certain range of normal angles (rather than at a fixed normal angle). Nevertheless, our calculations have taken into account the trend that the wave normal angles move toward 90° with the latitude increasing and the obtained results should qualitatively represent the latitudinal dependence of the growth rates of waves of different frequencies.

4. Propagation and Amplification of Magnetosonic Waves

To understand the propagation and path-integrated amplification of magnetosonic waves, we perform the backward ray-tracing simulations from the location of Probe A at 19:30 UT. We determine the ray trajectories using the code of Kimura (1966) and calculate the local growth rates K_i and then path-integrated gains G using our previously developed code (N. Liu et al., 2018a, 2018b; Su et al., 2018). We have terminated the ray-tracing simulations when $|K_i/K_r| > 0.01$ (with the cold plasma wavenumber K_r). Such singular points with $|K_i/K_r| > 0.01$ may correspond to the situation with the wave normal angles too close to 90° and the wave frequencies extremely close to the local proton gyrofrequency harmonics (Chen, 2015). The background magnetic field is simply assumed to be the typical dipole field, with a $\sim 10\%$ difference from the observation at the location of Probe A ($\lambda = 14.3^\circ$). The azimuthal variation of cold electron density has been ignored expediently, and the distribution of cold electron density in the meridian plane is modeled with the technique of Bortnik, Chen, et al. (2011). This model well reproduces the observed density profiles of the Van Allen Probes (Figure 3a) and exhibits the similar latitudinal dependence as described by Equation 1 (Figure S2). In our calculations (Figure 3a), the rays are found to migrate mainly within a relatively narrow range of $L \sim 5\text{--}6$ (Chen & Thorne, 2012; Gulelmi et al., 1975; Kasahara et al., 1994) and their azimuthal drifts are restricted to be within 2 h of the magnetic local time (MLT) away from the observer. In this limited computational domain, the hot proton distributions are assumed to depend on the latitude only. According to Liouville's theorem, the hot protons observed by Probe A at 19:30 UT ($\lambda = 14.3^\circ$) are mapped to other latitudes along the field lines. At latitudes below the observer, the smooth cubic spline extrapolation is used to estimate the proton phase space density near 90° pitch angle from the available measurements.

We have launched waves in the frequency f range from 50 to 260 Hz, with interval spacing at every 15 Hz. At each frequency, we have initialized waves of the backward normal angles $\psi_{\text{BW}} = 180^\circ - \psi \in [84^\circ, 96^\circ]$ with 0.5° spacing and of the backward azimuthal angles $\varphi_{\text{BW}} = \varphi - 180^\circ \in [-180^\circ, 0^\circ]$ with 3° spacing. The computational domain of ψ is generally consistent with the observations (Figure 1), and given the potentially significant error of φ derived from observations, its computational domain has been expanded to cover all the possible values in the azimuthally symmetric environment. We record the “maximum gain” $G_{\text{max}}(f, \psi_{\text{BW}}, \varphi_{\text{BW}}) = \max\{G(t, f, \psi_{\text{BW}}, \varphi_{\text{BW}}), t \in [0, t_e]\}$ for each ray during its propagation from the beginning $t = 0$ to the end $t = t_e$ (as exemplified in Figures 3b–3e), and then define the “super gain” $G_{\text{sup}}(f) = \max\{G_{\text{max}}(f, \psi_{\text{BW}}, \varphi_{\text{BW}}), \psi_{\text{BW}} \in [84^\circ, 96^\circ], \varphi_{\text{BW}} \in [-180^\circ, 0^\circ]\}$ at each frequency. For higher-frequency waves, the super gains tend to occur when the initial ψ_{BW} deviating more significantly from 90° at $\lambda = 14.3^\circ$. In other words, the substantial amplification of waves at higher frequencies requires contributions of ion instabilities at higher latitudes (Figure 2). The super gain reaches the peak of ~ 110 dB around 170 Hz and gradually decreases toward both frequency flanks (Figure 3f). The modeled super gain has an analogous frequency dependence to the observed wave power, seemingly supporting the possibility of accumulative amplification of the unusual magnetosonic waves over broad latitudes.

To understand the dependence of wave gain on the frequency and propagation angles, we compare the trajectories of waves launched with different values of f , ψ_{BW} , and φ_{BW} in Figure 4. The $f = 170$ Hz wave initialized with $\psi_{\text{BW}} = 93.5^\circ$ and $\varphi_{\text{BW}} = -87.0^\circ$ has an integrated gain of ~ 110 dB within 150 s. This wave ray is trapped near the plasmopause, bounces between latitudes of $\pm 30^\circ$, and drifts azimuthally toward the noonside. This wave gains energy mostly in the off-equatorial region $\lambda > 15^\circ$ with the normal angles close to 90° (see the zoom-in view of Figure S3). As this wave passes through the equator with the normal angles far away from 90° , it is amplified little or even damped. When the initial ψ_{BW} decreases to 92.0° , the wave has a limited amplification before experiencing the lower hybrid resonance (e.g., Horne, Wheeler, & Alleyne, 2000; Xiao, Zhou, et al., 2012). When the initial ψ_{BW} increases to 94.5° , the wave drifts azimuthally faster, bounces fewer rounds in the restricted MLT range, and then acquires less energy from the hot protons. Similarly, the decrease of initial φ_{BW} enlarges the range of radial migration, increases the time-averaged azimuthal drift velocity, and tends to reduce the wave gain. As for the wave at a lower frequency of $f = 95$ Hz, it prefers to grow in the region with a high Alfvén velocity, that is at low L -shells, in the plasmopause boundary layer or at relatively high latitudes. The wave initialized with a ψ_{BW} closer to 90° and a lower φ_{BW} migrates over a broader radial range and acquires more energy at low L -shells and in the plasmopause boundary layer. In contrast, an initial ψ_{BW} close to 90° is not conducive for the wave to reach relatively high latitudes and gain energy from the off-equatorial hot protons. Meanwhile, the azimuthal drift velocity

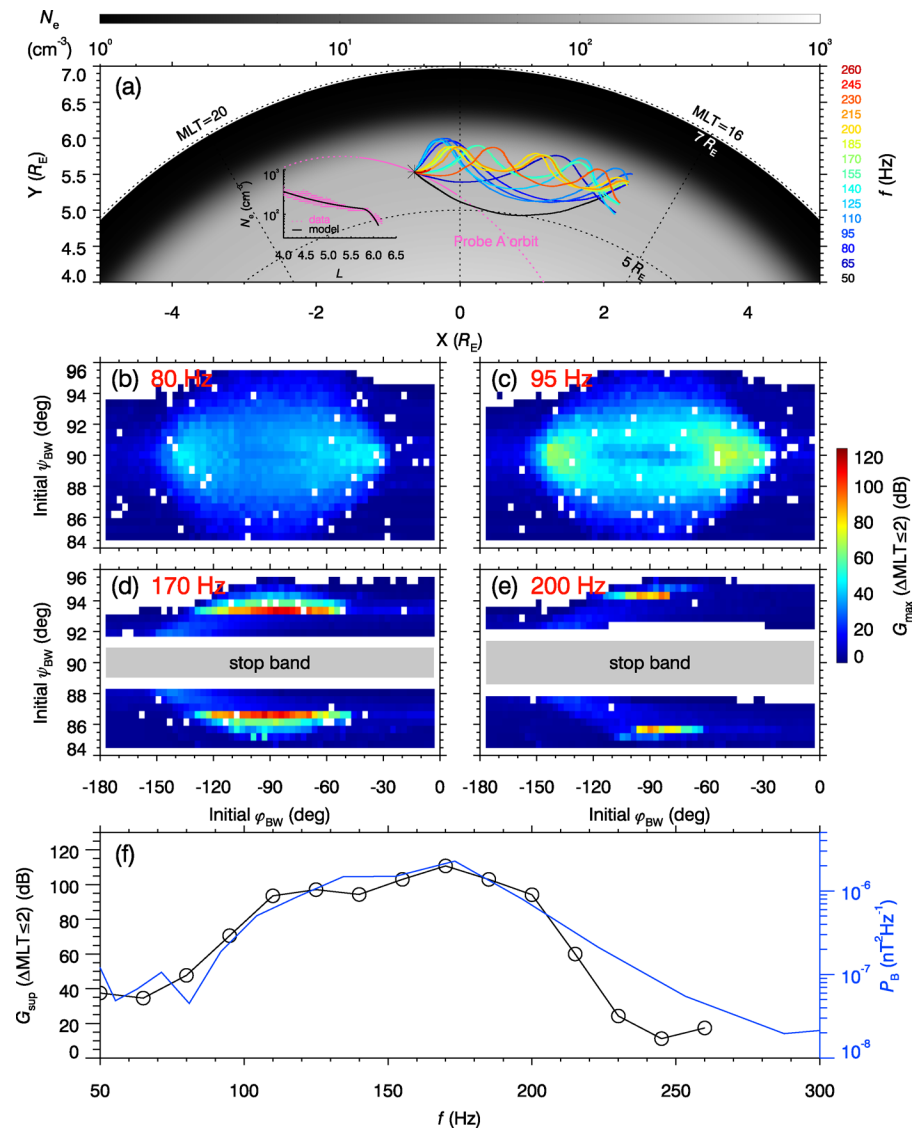


Figure 3. Path-integrated gains of 50–260 Hz waves from backward ray-tracing simulations: (a) modeled equatorial distribution of the cold electron density N_e in gray scale, with the overplotted orbit of Probe A mapped to the equator along the field lines (magenta solid line for 19:00–20:00 UT and magenta dashed line for 18:00–19:00 UT and 20:00–21:00 UT), the mapped trajectories of rays (color-coded according to the wave frequency) initialized at the “optimal” propagation angles to reach the super gain, and the superimposed data-to-model comparison of radial profiles of cold electron density; dependence of (b) 80 Hz, (c) 95 Hz, (d) 155 Hz, (e) 200 Hz wave maximum gain G_{\max} (color-coded) on the initial ψ_{BW} and φ_{BW} , with the gray shadow for the stop band of the cold-plasma wave dispersion relation and the blank region for the negative values or related to the singular points; (f) frequency-dependence of the modeled super gain G_{sup} (black) and the observed magnetic power spectral density P_B (blue) from Probe A at 19:30 UT.

controlled by the initial ψ_{BW} and φ_{BW} also affects the final gain. A competition among these factors explains the dependence of 95 Hz wave gain on the initial propagation angles.

5. Discussion

In the analyses above, we have assumed the waves are propagating in the fast magnetosonic mode of the cold-plasma dispersion relation. K. Liu et al. (2011) and Min and Liu (2015) have demonstrated that the dispersion relation will change from the fast magnetosonic mode to the ion Bernstein mode when the proportion of ring-like distributed hot protons density increases to a considerably high level ($N_p/N_e > 0.1$). For

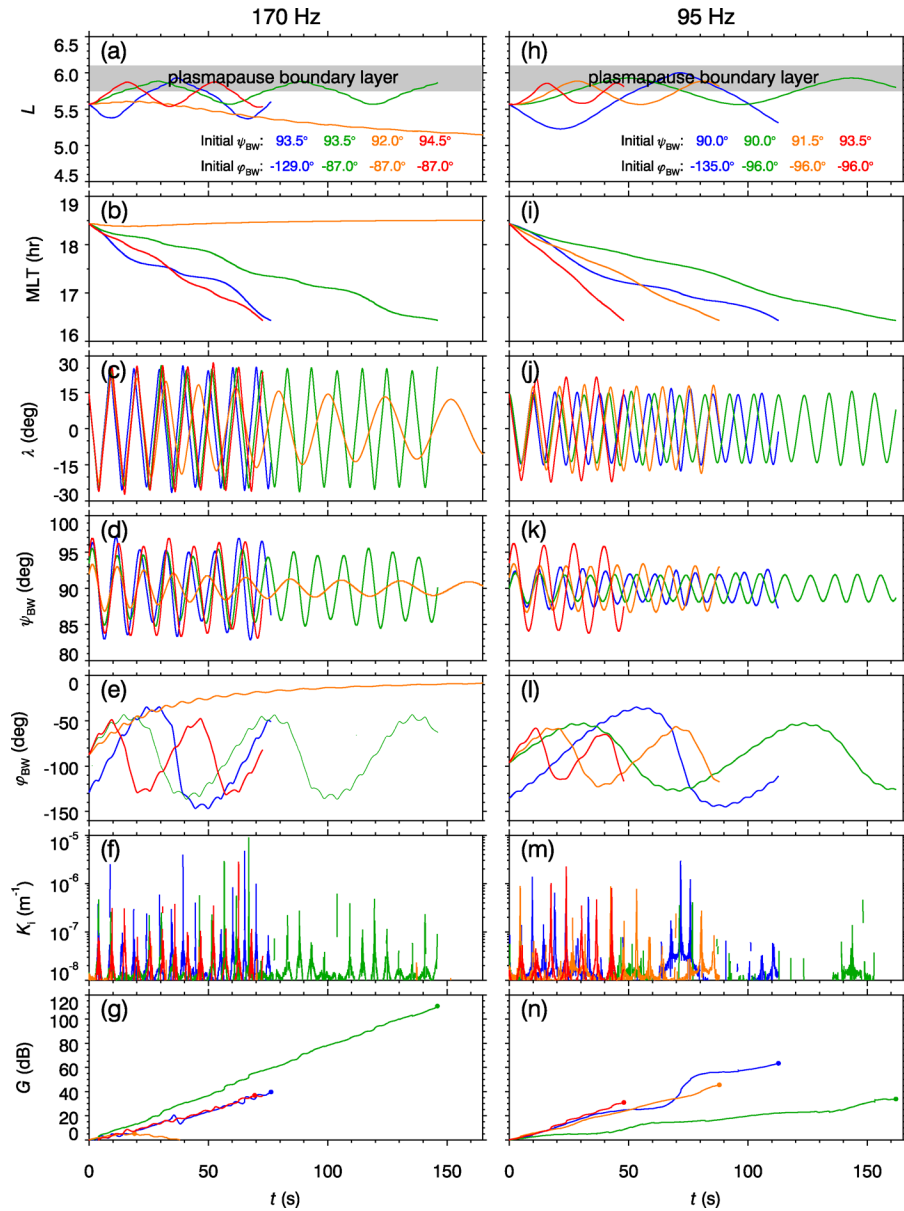


Figure 4. Temporal evolution of 170 Hz (left) and 95 Hz (right) rays: (a and h) L -shell; (b and i) magnetic local time MLT; (c and j) magnetic latitude λ ; (d and k) backward normal angle ψ_{BW} ; (e and l) backward azimuthal angle ϕ_{BW} ; (f and m) convective growth rate K_i ; (g and n) path-integrated gain G , with the dot marking the maximum value for each ray. Colors help differentiate among the results with different initial ψ_{BW} and ϕ_{BW} (indicated).

the event of interest in the high-density plasmasphere, the proportion of hot protons above $E_k = 30$ eV was lower than 0.01 (Figure S4), more than one order of magnitude smaller than the proposed threshold for the dispersion relation transformation (Min & Liu, 2015). Therefore, our assumption of the cold plasma dispersion relation may still be reasonable (Figure 1 of Chen et al., 2016).

Our results suggest the off-equatorial generation of magnetosonic waves observed by Van Allen Probes in the duskside plasmasphere during the outbound pass (Figure 1). During the subsequent inbound pass (Figure S5), the Van Allen Probes detected again the magnetosonic waves extending above the lower hybrid resonance frequency at $\lambda \approx 12^\circ$ in the nightside plasmasphere. Probably due to the enhanced hot proton injections, the power of the inbound magnetosonic waves was more than one order of magnitude larger than that of the outbound waves. These observations imply that such off-equatorially generated magnetosonic

waves could last 5 h or more over a broad radial and azimuthal range. We speculate that strong proton rings may produce such magnetosonic waves in the outer plasmasphere. A sufficiently strong proton ring allows the growth of waves over a broad range of latitudes, and the near-plasmapause trapping (Chen & Thorne, 2012; Gulelmi et al., 1975; Kasahara et al., 1994) favors their repeated growth over a broad range of magnetic local times.

The proposed generation mechanism here is based on the linear instability theory, essentially different from the nonlinear wave-wave interaction mechanism to generate magnetosonic waves beyond the lower hybrid resonance frequency in the magnetotail (Huang et al., 2020). Our mechanism is also a plausible candidate to explain other off-equatorial magnetosonic waves below the lower hybrid resonance frequency (e.g., Boardsen, Hospodarsky, Kletzing, et al., 2016; Ni et al., 2018; Tsurutani et al., 2014; Zhima et al., 2015). With appropriate distributions of hot protons, the central frequency of magnetosonic waves generated in the off-equatorial region might move toward the low-frequency end. Because of the bounce motions, all these waves should be observable over a broad range of latitudes. By analyzing ~ 1 year of wave data from Polar spacecraft, Tsurutani et al. (2014) have found the magnetosonic waves occur over the latitudes λ from -60° to 20° and $\sim 10\%$ of the wave events emerge at the off-equatorial latitudes of $|\lambda| > 15^\circ$. As shown in our simulation, the superimposed contributions of ion Bernstein instabilities over a broad range of latitudes have smeared out the sharp harmonic structures. Tsurutani et al. (2014) have reported the large-amplitude (~ 1 nT) magnetosonic waves without clear harmonic structures at the equator. The extreme intensity of waves may be attributed to the accumulative linear growth over a broad range of latitudes and magnetic local times with extremely strong proton rings or the additional nonlinear growth, by analogy with whistler-mode chorus waves (Omura et al., 2008).

There have been mainly three mechanisms proposed for magnetosonic waves to affect the radiation belt electron dynamics: Landau resonance (Horne, Thorne, et al., 2007), bounce resonance (Shprits, 2009), and transit-time scattering (Bortnik & Thorne, 2010). The range and efficiency of Landau and bounce resonances are sensitive to the wavevector distribution and the background parameters (X. Li et al., 2015; J. Li et al., 2016; Maldonado & Chen, 2018; Ni et al., 2018; Xiao, Yang, et al., 2015), and the transit-time scattering is favored by the limited latitudinal coverage (Bortnik & Thorne, 2010; Bortnik, Thorne, Ni, & Li, 2015; Yu et al., 2020). Compared to the near-equatorially generated magnetosonic waves, the off-equatorially generated waves cover a broader latitudinal range and have the wavevectors deviating more significantly from the perpendicular direction at low latitudes. Therefore, these magnetosonic waves of distinct sources may have quite different effects on the radiation belt electrons.

6. Summary

Magnetosonic waves are commonly considered to be generated below the lower hybrid resonance frequency near the magnetic equator in the inner magnetosphere. In this letter, we present the unusual observations of magnetosonic waves substantially extending above the local lower hybrid resonance frequency in the off-equatorial plasmasphere. These unusual magnetosonic waves are found to be closely related to the sub-storm injection of hot protons and roughly bounded between the lower hybrid resonance frequencies at the equator and at the latitude of 25° . We evaluate the linear growth rates of magnetosonic waves for the observed hot proton distributions at different latitudes along the magnetic field lines. According to the cold-plasma wave dispersion relation, the allowed propagation cone for these high frequency waves deviates more significantly from the perpendicular direction at lower latitudes with weaker magnetic fields. In our simulation, the equatorial growth of magnetosonic waves at normal angles far from 90° is quite weak. In contrast, as the allowed normal angles move close to 90° at relatively high latitudes ($>15^\circ$), the magnetosonic waves could grow at a high rate beyond 10^{-6} m^{-1} . Moreover, on the basis of available data, we construct an idealized model to investigate the propagation and path-integrated amplification of magnetosonic waves. At each frequency, we determine the super gain among waves initialized with different propagation angles. With the appropriate propagation angles, these waves accumulatively gain energy from the hot protons over latitudes $|\lambda| < 30^\circ$ during the bounce-drift process inside the plasmasphere. The effective amplification of waves at higher frequencies tends to require contributions of ion instabilities at higher latitudes. The modeled super gain reaches a peak of ~ 110 dB around the central frequency and decreases gradually toward both frequency flanks, seemingly responsible for the observed frequency-dependence of magnetosonic wave

power. Our data and modeling illustrate a previously unexplored scenario that off-equatorial proton ring distributions could be a significant source of magnetosonic waves in the inner magnetosphere. Because of the differences in the latitudinal coverage and wavevector distribution, the off-equatorially generated magnetosonic waves would affect the radiation belt electrons in a quite different way from the equatorially generated ones.

Data Availability Statement

Van Allen Probes data are obtained from the following websites: <http://emfisis.physics.uiowa.edu/Flight/>, http://www.rbsp-ect.lanl.gov/data_pub/, and <http://rbspice.ftccs.com/>. Geomagnetic indices are obtained from the website: <http://wdc.kugi.kyoto-u.ac.jp>. Ray-tracing code is obtained from the website: <http://waves.is.t.kanazawa-u.ac.jp/>.

Acknowledgments

The authors acknowledge EMFISIS, ECT, and RBSPICE teams for the use of Van Allen Probes data and acknowledge Iwane Kimura for the use of ray-tracing code. This work was supported by the Strategic Priority Research Program of Chinese Academy of Sciences grant XDB 41000000, the National Natural Science Foundation of China grants 41774170 and 41631071, the Chinese Academy of Sciences grant KZCX2-EW-QN510 and KZZD-EW-01-4, the CAS Key Research Program of Frontier Sciences grant QYZDB-SSW-DQC015, the National Key Basic Research Special Foundation of China Grant No. 2011CB811403, the National Postdoctoral Program for Innovative Talents Grant BX20190310, the China Postdoctoral Science Foundation Grant No. 2019M662171, and the Fundamental Research Funds for the Central Universities WK2080000005.

References

- Boardsen, S. A., Gallagher, D. L., Gurnett, D. A., Peterson, W. K., & Green, J. L. (1992). Funnel-shaped, low-frequency equatorial waves. *Journal of Geophysical Research*, 97, 14. <https://doi.org/10.1029/92JA00827>
- Boardsen, S. A., Hospodarsky, G. B., Kletzing, C. A., Engebretson, M. J., Pfaff, R. F., Wygant, J. R., & De Pascuale, S. (2016). Survey of the frequency dependent latitudinal distribution of the fast magnetosonic wave mode from Van Allen Probes Electric and Magnetic Field Instrument and Integrated Science waveform receiver plasma wave analysis. *Journal of Geophysical Research: Space Physics*, 121, 2902–2921. <https://doi.org/10.1002/2015JA021844>
- Boardsen, S. A., Hospodarsky, G. B., Min, K., Averkamp, T. F., Bounds, S. R., Kletzing, C. A., & Pfaff, R. F. (2018). Determining the wave vector direction of equatorial fast magnetosonic waves. *Geophysical Research Letters*, 45(16), 7951–7959. <https://doi.org/10.1029/2018GL078695>
- Bortnik, J., Chen, L., Li, W., Thorne, R. M., & Horne, R. B. (2011). Modeling the evolution of chorus waves into plasmaspheric hiss. *Journal of Geophysical Research*, 116, 8221. <https://doi.org/10.1029/2011JA016499>
- Bortnik, J., & Thorne, R. M. (2010). Transit time scattering of energetic electrons due to equatorially confined magnetosonic waves. *Journal of Geophysical Research*, 115, A07213. <https://doi.org/10.1029/2010JA015283>
- Bortnik, J., Thorne, R. M., Ni, B., & Li, J. (2015). Analytical approximation of transit time scattering due to magnetosonic waves. *Geophysical Research Letters*, 42(5), 1318–1325. <https://doi.org/10.1002/2014GL062710>
- Chen, L. (2015). Wave normal angle and frequency characteristics of magnetosonic wave linear instability. *Geophysical Research Letters*, 42(12), 4709–4715. <https://doi.org/10.1002/2015GL064237>
- Chen, L., Sun, J., Lu, Q., Gao, X., Xia, Z., & Zhima, Z. (2016). Generation of magnetosonic waves over a continuous spectrum. *Journal of Geophysical Research: Space Physics*, 121, 1137–1147. <https://doi.org/10.1002/2015JA022089>
- Chen, L., & Thorne, R. M. (2012). Perpendicular propagation of magnetosonic waves. *Geophysical Research Letters*, 39, L14102. <https://doi.org/10.1029/2012GL052485>
- Chen, L., Thorne, R. M., Jordanova, V. K., & Horne, R. B. (2010). Global simulation of magnetosonic wave instability in the storm time magnetosphere. *Journal of Geophysical Research*, 115(A11), A11222. <https://doi.org/10.1029/2010JA015707>
- Curtis, S. A., & Wu, C. S. (1979). Gyroharmonic emissions induced by energetic ions in the equatorial plasmasphere. *Journal of Geophysical Research*, 84, 2597–2607. <https://doi.org/10.1029/JA084iA06p02597>
- De Boor, C. (1977). Package for calculating with B-splines. *SIAM Journal on Numerical Analysis*, 14(3), 441–472.
- Denton, R. E., Goldstein, J., & Menietti, J. D. (2002). Field line dependence of magnetospheric electron density. *Geophysical Research Letters*, 29(24), 2205. <https://doi.org/10.1029/2002GL015963>
- Funsten, H. O., Skoug, R. M., Guthrie, A. A., MacDonald, E. A., Baldonado, J. R., Harper, R. W., et al. (2013). Helium, Oxygen, Proton, and Electron (HOPE) mass spectrometer for the radiation belt storm probes mission. *Space Science Reviews*, 179, 423–484. <https://doi.org/10.1007/s11214-013-9968-7>
- Gary, S. P., Liu, K., Winske, D., & Denton, R. E. (2010). Ion Bernstein instability in the terrestrial magnetosphere: Linear dispersion theory. *Journal of Geophysical Research*, 115, A12209. <https://doi.org/10.1029/2010JA015965>
- Gulelmi, A. V., Klaine, B. I., & Potapov, A. S. (1975). Excitation of magnetosonic waves with discrete spectrum in the equatorial vicinity of the plasmapause. *Planetary and Space Science*, 23, 279–286. [https://doi.org/10.1016/0032-0633\(75\)90133-6](https://doi.org/10.1016/0032-0633(75)90133-6)
- Horne, R. B., Thorne, R. M., Glauert, S. A., Meredith, N. P., Pokhotelov, D., & Santolík, O. (2007). Electron acceleration in the Van Allen radiation belts by fast magnetosonic waves. *Geophysical Research Letters*, 34, L17107. <https://doi.org/10.1029/2007GL030267>
- Horne, R. B., Wheeler, G. V., & Alleyne, H. S. C. K. (2000). Proton and electron heating by radially propagating fast magnetosonic waves. *Journal of Geophysical Research*, 105, 27597–27610. <https://doi.org/10.1029/2000JA000018>
- Huang, S. Y., Deng, D., Yuan, Z. G., Jiang, K., Li, J. X., Deng, X. H., & Xu, S. B. (2020). First observations of magnetosonic waves with non-linear harmonics. *Journal of Geophysical Research: Space Physics*, 125(6), e27724. <https://doi.org/10.1029/2019JA027724>
- Kasahara, Y., Kenmochi, H., & Kimura, I. (1994). Propagation characteristics of the ELF emissions observed by the satellite Akebono in the magnetic equatorial region. *Radio Science*, 29, 751–767. <https://doi.org/10.1029/94RS00445>
- Kennel, C. (1966). Low-frequency whistler mode. *Physics of Fluids*, 9, 2190–2202. <https://doi.org/10.1063/1.1761588>
- Kimura, I. (1966). Effects of ions on whistler-mode ray tracing. *Radio Science*, 1(3), 269–284. <https://doi.org/10.1002/rds196613269>
- Kistler, L. M., Mouikis, C. G., Spence, H. E., Menz, A. M., Skoug, R. M., Funsten, H. O., & Lanzerotti, L. J. (2016). The source of O⁺ in the storm time ring current. *Journal of Geophysical Research: Space Physics*, 121(6), 5333–5349. <https://doi.org/10.1002/2015JA022204>
- Kletzing, C. A., Kurth, W. S., Acuna, M., MacDowall, R. J., Torbert, R. B., Averkamp, T., & Tyler, J. (2013). The electric and magnetic field instrument suite and integrated science (EMFISIS) on RBSP. *Space Science Reviews*, 179, 127–181. <https://doi.org/10.1007/s11214-013-9993-6>
- Kurth, W. S., Pascuale, S. D., Faden, J. B., Kletzing, C. A., Hospodarsky, G. B., Thaller, S., & Wygant, J. R. (2014). Electron densities inferred from plasma wave spectra obtained by the waves instrument on Van Allen probes. *Journal of Geophysical Research: Space Physics*, 120, 904–914. <https://doi.org/10.1002/2014JA020857>

- Li, J., Ni, B., Ma, Q., Xie, L., Pu, Z., Fu, S., & Summers, D. (2016). Formation of energetic electron butterfly distributions by magnetosonic waves via Landau resonance. *Geophysical Research Letters*, *43*, 3009–3016. <https://doi.org/10.1002/2016GL067853>
- Li, X., Tao, X., Lu, Q., & Dai, L. (2015). Bounce resonance diffusion coefficients for spatially confined waves. *Geophysical Research Letters*, *42*(22), 9591–9599. <https://doi.org/10.1002/2015GL066324>
- Liu, K., Gary, S. P., & Winske, D. (2011). Excitation of magnetosonic waves in the terrestrial magnetosphere: Particle-in-cell simulations. *Journal of Geophysical Research*, *116*, A07212. <https://doi.org/10.1029/2010JA016372>
- Liu, N., Su, Z., Zheng, H., Wang, Y., & Wang, S. (2018a). Magnetosonic harmonic falling and rising frequency emissions potentially generated by nonlinear wave-wave interactions in the Van Allen radiation belts. *Geophysical Research Letters*, *45*(16), 7985–7995. <https://doi.org/10.1029/2018GL079232>
- Liu, N., Su, Z., Zheng, H., Wang, Y., & Wang, S. (2018b). Prompt disappearance and emergence of radiation belt magnetosonic waves induced by solar wind dynamic pressure variations. *Geophysical Research Letters*, *45*(2), 585–594. <https://doi.org/10.1002/2017GL076382>
- Ma, Q., Li, W., Bortnik, J., Kletzing, C. A., Kurth, W. S., Hospodarsky, G. B., & Wygant, J. R. (2019). Global survey and empirical model of fast magnetosonic waves over their full frequency range in Earth's inner magnetosphere. *Journal of Geophysical Research: Space Physics*, *124*(12), 10270–10282. <https://doi.org/10.1029/2019JA027407>
- Ma, Q., Li, W., Chen, L., Thorne, R. M., & Angelopoulos, V. (2014). Magnetosonic wave excitation by ion ring distributions in the Earth's inner magnetosphere. *Journal of Geophysical Research: Space Physics*, *119*(2), 844–852. <https://doi.org/10.1002/2013JA019591>
- Maldonado, A. A., & Chen, L. (2018). On the diffusion rates of electron bounce resonant scattering by magnetosonic waves. *Geophysical Research Letters*, *45*(8), 3328–3337. <https://doi.org/10.1002/2017GL076560>
- Mauk, B. H., Fox, N. J., Kanekal, S. G., Kessel, R. L., Sibeck, D. G., & Ukhorskiy, A. (2013). Science objectives and rationale for the radiation belt storm probes mission. *Space Science Reviews*, *179*, 3–27. <https://doi.org/10.1007/s11214-012-9908-y>
- Meredith, N. P., Horne, R. B., & Anderson, R. R. (2008). Survey of magnetosonic waves and proton ring distributions in the Earth's inner magnetosphere. *Journal of Geophysical Research*, *113*, A06213. <https://doi.org/10.1029/2007JA012975>
- Min, K., & Liu, K. (2015). Regime transition of ion Bernstein instability driven by ion shell velocity distributions. *Journal of Geophysical Research: Space Physics*, *120*(10), 8448–8454. <https://doi.org/10.1002/2015JA021514>
- Min, K., Liu, K., Wang, X., Chen, L., & Denton, R. E. (2018). Fast magnetosonic waves observed by Van Allen probes: Testing local wave excitation mechanism. *Journal of Geophysical Research: Space Physics*, *123*(1), 497–512. <https://doi.org/10.1002/2017JA024867>
- Mitchell, D. G., Lanzerotti, L. J., Kim, C. K., Stokes, M., Ho, G., Cooper, S., & Kerem, S. (2013). Radiation Belt Storm Probes Ion Composition Experiment (RBSPICE). *Space Science Reviews*, *179*(1–4), 263–308. <https://doi.org/10.1007/s11214-013-9965-x>
- Němec, F., Santolik, O., Gereová, K., Macúšová, E., de Conchy, Y., & Cornilleau-Wehrlin, N. (2005). Initial results of a survey of equatorial noise emissions observed by the Cluster spacecraft. *Planetary and Space Science*, *53*, 291–298. <https://doi.org/10.1016/j.pss.2004.09.055>
- Ni, B., Zou, Z., Fu, S., Cao, X., Gu, X., & Xiang, Z. (2018). Resonant scattering of radiation belt electrons by off-equatorial magnetosonic waves. *Geophysical Research Letters*, *45*(3), 1228–1236. <https://doi.org/10.1002/2017GL075788>
- Omura, Y., Katoh, Y., & Summers, D. (2008). Theory and simulation of the generation of whistler-mode chorus. *Journal of Geophysical Research*, *113*(A12), 4223. <https://doi.org/10.1029/2007JA012622>
- Perraut, S., Roux, A., Robert, P., Gendrin, R., Sauvaud, J.-A., Bosqued, J.-M., & Korth, A. (1982). A systematic study of ULF waves above from GEOS 1 and 2 measurements and their relationships with proton ring distributions. *Journal of Geophysical Research*, *87*, 6219–6236. <https://doi.org/10.1029/JA087iA08p06219>
- Reinsch, C. H. (1967). Smoothing by spline functions. *Numerische Mathematik*, *10*(3), 177–183.
- Russell, C. T., Holzer, R. E., & Smith, E. J. (1970). OGO 3 observations of ELF noise in the magnetosphere. 2. The nature of the equatorial noise. *Journal of Geophysical Research*, *75*, 755–768. <https://doi.org/10.1029/JA075i004p00755>
- Santolik, O., Parrot, M., & Lefeuvre, F. (2003). Singular value decomposition methods for wave propagation analysis. *Radio Science*, *38*, 1010. <https://doi.org/10.1029/2000RS002523>
- Santolik, O., Parrot, M., & Němec, F. (2016). Propagation of equatorial noise to low altitudes: Decoupling from the magnetosonic mode. *Geophysical Research Letters*, *43*, 6694–6704. <https://doi.org/10.1002/2016GL069582>
- Santolik, O., Pickett, J. S., Gurnett, D. A., Maksimovic, M., & Cornilleau-Wehrlin, N. (2002). Spatiotemporal variability and propagation of equatorial noise observed by Cluster. *Journal of Geophysical Research*, *107*, 1495. <https://doi.org/10.1029/2001JA009159>
- Santolik, O., Pickett, J. S., Gurnett, D. A., & Storey, L. R. O. (2002). Magnetic component of narrowband ion cyclotron waves in the auroral zone. *J. Geophys. Res. Space Physics*, *107*, 1444. <https://doi.org/10.1029/2001JA000146>
- Shprits, Y. Y. (2009). Potential waves for pitch-angle scattering of near-equatorially mirroring energetic electrons due to the violation of the second adiabatic invariant. *Geophysical Research Letters*, *36*, L12106. <https://doi.org/10.1029/2009GL038322>
- Spence, H. E., Yang, C., He, Z., Su, Z., Zhou, Q., He, Y., & Wygant, J. R. (2013). Science goals and overview of the energetic particle, composition, and thermal plasma (ECT) suite on NASAs Radiation Belt Storm Probes (RBSP) mission. *Space Science Reviews*, *179*, 311–336. <https://doi.org/10.1007/s11214-013-0007-5>
- Stix, T. H. (1962). *The theory of plasma waves*. New York, NY: McGraw-hill.
- Su, Z., Liu, N., Zheng, H., Wang, Y., & Wang, S. (2018). Large-amplitude extremely low frequency hiss waves in plasmaspheric plumes. *Geophysical Research Letters*, *45*(2), 565–577. <https://doi.org/10.1002/2017GL076754>
- Su, Z., Wang, G., Liu, N., Zheng, H., Wang, Y., & Wang, S. (2017). Direct observation of generation and propagation of magnetosonic waves following substorm injection. *Geophysical Research Letters*, *44*(15), 7587–7597. <https://doi.org/10.1002/2017GL074362>
- Tsurutani, B. T., Falkowski, B. J., Pickett, J. S., Verkhoglyadova, O. P., Santolik, O., & Lakhina, G. S. (2014). Extremely intense ELF magnetosonic waves: A survey of polar observations. *Journal of Geophysical Research: Space Physics*, *119*, 964–977. <https://doi.org/10.1002/2013JA019284>
- Tsyganenko, N. A., & Sitnov, M. I. (2005). Modeling the dynamics of the inner magnetosphere during strong geomagnetic storms. *Journal of Geophysical Research*, *110*, A03208. <https://doi.org/10.1029/2004JA010798>
- Xiao, F., Yang, C., Su, Z., Zhou, Q., He, Z., He, Y., & Blake, J. B. (2015). Wave-driven butterfly distribution of Van Allen belt relativistic electrons. *Nature Communications*, *6*, 8590. <https://doi.org/10.1038/ncomms9590>
- Xiao, F., Zhou, Q., He, Z., & Tang, L. (2012). Three-dimensional ray tracing of fast magnetosonic waves. *Journal of Geophysical Research*, *117*(A6), A06208. <https://doi.org/10.1029/2012JA017589>
- Yu, X., Yuan, Z., & Yu, J. (2020). Revisit the analytical approximation of transit-time scattering for fast magnetosonic waves. *Geophysical Research Letters*, *47*(16), e88434. <https://doi.org/10.1029/2020GL088434>

- Yuan, Z., Yao, F., Yu, X., Huang, S., & Ouyang, Z. (2019). An Automatic Detection Algorithm Applied to Fast Magnetosonic Waves With Observations of the Van Allen Probes. *Journal of Geophysical Research*, *124*(5), 3501–3511. <https://doi.org/10.1029/2018JA026387>
- Zhima, Z., Chen, L., Fu, H., Cao, J., Horne, R. B., & Reeves, G. (2015). Observations of discrete magnetosonic waves off the magnetic equator. *Geophysical Research Letters*, *42*(22), 9694–9701. <https://doi.org/10.1002/2015GL066255>